Topological properties and self-energy effects in elemental Yb

P. M. Sheverdyaeva,[1,*] F. Offi,[2] S. Gardonio,[3] L. Novinec,[3,†] M. I. Trioni,[4] D. Ceresoli,[4] S. Iacobucci,[5] A. Ruocco,[2] G. Stefani,[5] L. Petaccia,[6] S. Gorovikov,[6,‡] E. Cappelluti,[1] P. Moras,[1] G. Bihlmayer,[7,§] S. Blügel,[7] and C. Carbone[1]

[1]*Istituto di Struttura della Materia-CNR (ISM-CNR), I-34149 Trieste, Italy*
[2]*Dipartimento di Scienze, Università degli Studi Roma Tre, I-00146 Rome, Italy*
[3]*Materials Research Laboratory, University of Nova Gorica, 5000 Nova Gorica, Slovenia*
[4]*Istituto SCITEC "Giulio Natta," Consiglio Nazionale delle Ricerche, I-20133 Milano, Italy*
[5]*Istituto di Struttura della Materia (ISM-CNR), Area della Ricerca di Roma 2 Tor Vergata, Via Fosso del Cavaliere 100, 00133 Roma, Italy*
[6]*Elettra Sincrotrone Trieste, Strada Statale 14 km 163.5, 34149 Trieste, Italy*
[7]*Peter Grünberg Institut and Institute for Advanced Simulation, Forschungszentrum Jülich and JARA, 52425 Jülich, Germany*

(Received 30 August 2021; accepted 3 November 2021; published 19 November 2021)

Recent theoretical calculations predict the presence of Dirac nodal lines with π Berry phase and related topological surface states in elemental alkaline-earth metals. Here we provide experimental and theoretical evidence for the existence of similar nodal lines also in hexagonal close-packed Yb, an element of the lanthanide series, in the limit of zero spin-orbit coupling. These topological properties emerge after taking into account self-energy corrections, which permit one to correctly describe the experimental low-energy electronic structure of Yb. By angle-resolved photoemission spectroscopy we demonstrate the occurrence of topological surface states in Yb which are robust in the presence of the large spin-orbit coupling.

DOI: 10.1103/PhysRevB.104.195138

I. INTRODUCTION

Dirac nodal lines (DNLs) are topological features in the band structure which attracted great attention in recent years. In a DNL material the crossing of conduction and valence bands forms a closed path in the momentum space [1]. The topological nature of the DNLs can give rise to several phenomena, such as robust topological surface states (TSSs), a nontrivial Berry phase, and the spin Hall effect [1–4]. Among the elemental materials, the alkaline-earth metals Be and Mg, with hexagonal close-packed (hcp) structure, and Ca and Sr, with face-centered cubic structure (fcc), were predicted to have DNLs with a π Berry phase near the Fermi level in the limit of vanishing spin-orbit coupling (SOC) [2,5]. The existence of DNLs and TSSs was demonstrated to explain many exotic properties of alkaline-earth metals, such as anomalously high electron-phonon coupling [6], giant Friedel oscillations [7], and a semimetal-semiconductor transition [8,9]. An experimental verification of the theoretical predictions was limited to the Be(0001) surface, where the projection of the DNL as well as a circular contour, related to a TSS, were experimentally observed by angle-resolved photoemission spectroscopy (ARPES) [5,10].

Yb is a divalent lanthanide metal with a filled $4f$ shell and close-packed structure at ambient conditions, which shares a number of properties with alkaline-earth metals, including a similar chemical behavior, semimetal-semiconductor transition under pressure [9,11], and pressure-induced superconductivity [12]. Close to room temperature Yb was reported to exist in both fcc and hcp structures [13–16]. Similarly to alkaline-earth metals, fcc Yb was predicted to possess a DNL, which becomes gapped due to the large SOC of Yb [2] and may give origin to a large spin Hall conductivity [3,4]. The existence of DNL in hcp Yb has not yet been addressed. So far, many of the properties of Yb remain not fully understood due to a discrepancy between the experimental and theoretical electronic band structures. Photoemission spectroscopy on close-packed Yb surfaces presents a peaked density of states close to the Fermi level [17–24]. Resistivity and Hall data on bulk Yb [14,25] and scanning tunneling spectroscopy on thin Yb films grown on W(110) [26,27] suggest the existence of an electron pocket at the center of the surface Brillouin zone ($\overline{\Gamma}$). Instead, band structure calculations do not reproduce this pocket and indicate a semimetallic behavior for both hcp and fcc structures [11,24,25,28–32].

With the aim of clarifying the electronic structure of Yb close to the Fermi level, we performed a joint density functional theory (DFT) and ARPES investigation on Yb(0001) thin films grown on Mo(110). ARPES reveals the existence of an electron pocket at $\overline{\Gamma}$ in hcp Yb. We demonstrate that this pocket can be reproduced in DFT by including self-energy corrections via a Hubbard U correction on the empty d orbitals. The same correction induces a similar pocket also in fcc Yb. Within this approach we show the formation of two concentric DNLs with $\pm\pi$ Berry phase and related TSSs in the electronic structure of hcp Yb. We furthermore provide an ARPES evidence for these TSSs. Our revision of the

*Corresponding author: polina.sheverdyaeva@ism.cnr.it
†Present address: Elettra Sincrotrone Trieste, Strada Statale 14 km 163.5, 34149 Trieste, Italy.
‡Present address: Canadian Light Source Inc., 44 Innovation Boulevard, S7N 2V3 Saskatoon, SK, Canada.
§Corresponding author: g.bihlmayer@fz-juelich.de

low-energy electronic structure of Yb calls for a reinterpretation of the electronic and transport properties and for the exploration of novel phenomena in this material.

II. METHODS

The ARPES experiments were performed at the VUV-Photoemission and BaDElPh [33] beamlines at the Elettra synchrotron radiation facility in Trieste, Italy. Photoelectron spectra were recorded at room temperature with a total instrumental energy resolution of 10 meV and an angular resolution of 0.25° at different photon energies ranging from 6 eV up to 40 eV. The Mo(110) surface was cleaned by repeated high-temperature flash-annealing cycles in oxygen atmosphere up to 2000 K, until low-energy electron diffraction (LEED) and x-ray photoelectron spectroscopy indicated a clean and ordered surface. Yb was deposited at room temperature by electron-beam evaporation from a Ta crucible using a deposition rate of about 5 Å/min. The base pressure of the experimental station rose from 1×10^{-10} mbar to 1×10^{-9} mbar during Yb deposition. A quartz microbalance was used to monitor the thickness of the deposited film. The evaporation rate was cross-checked by monitoring the Yb $4f$ core level [34,35]. The deposition of Yb on Mo(110) at room temperature in the investigated thickness range of 4–60 ML (monolayer) leads to a well-ordered epitaxial film having a hexagonal (1×1) LEED pattern.

We calculated the electronic structure of the different Yb phases using the full-potential linearized augmented plane-wave method as implemented in the FLEUR code [36], based on density functional theory with the exchange-correlation potential in the generalized gradient approximation [37]. The $5s$ and $5p$ orbitals of Yb were treated as local orbitals and the DFT+U method in the fully localized limit was employed for the $4f$ states with $U_f = 6.0$ eV and $J_f = 0.7$ eV. Where mentioned, also the $5d$ orbitals were treated with the DFT+U method in the fully localized limit using $U_d = 4.0$ eV and $J_d = 0.7$ eV, and spin-orbit coupling was included in a self-consistent manner. A product of wave-function cutoff times muffin-tin radius of 11.2 and optimized lattice parameters of $a_{hex} = 3.852$ Å and $c/a = 1.633$ with an $8 \times 8 \times 4$ k-point set for the hcp bulk phase ($8 \times 8 \times 8$ for fcc) were used. The films were set up containing 24 closed-packed layers embedded in vacuum [38] showing negligible relaxations of the surface layers ($< 0.4\%$). For the calculation of the Berry curvatures we constructed Wannier functions for the (s,p,d) orbitals and used the WANNIERTOOLS code [39].

III. RESULTS AND DISCUSSION

Figure 1(a) reports ARPES data for thin Yb films on Mo(110). We notice the presence of quantum well states (QWSs) with paraboliclike dispersion centered around $\overline{\Gamma}$, whose number increases with the film thickness (1 ML = 3.1 Å [40]). These states arise from the spatial confinement of the electron wave functions within the films and correspond to the discretization of the electron momentum perpendicular to the surface of a bulk Yb band. The bottom edge of this band at $\overline{\Gamma}$ can be easily determined as the position of the deepest QWS for sufficiently thick films [Fig. 1(b)], as

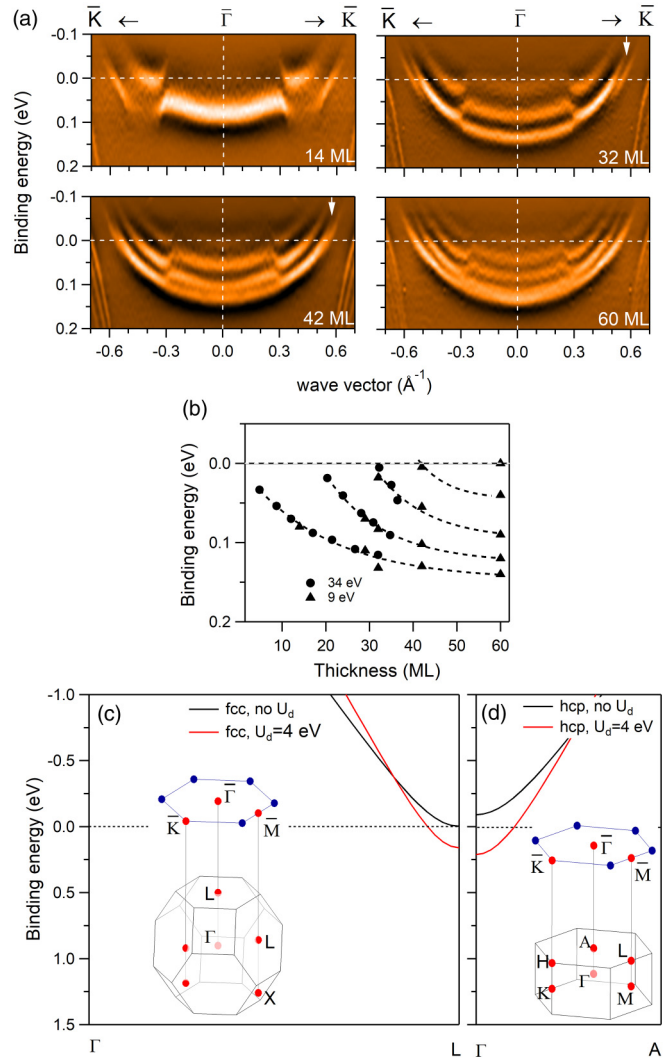

FIG. 1. (a) ARPES maps taken with $h\nu = 9$ eV at room temperature along $\overline{K}\,\overline{\Gamma}\,\overline{K}$ direction and around E_F for different thicknesses as indicated. The images are taken around the $\overline{\Gamma}$ point, normalized to the Fermi function and in a form of second derivative. (b) Energy position versus film thickness of the bands at the $\overline{\Gamma}$ point represented by solid symbols (circles for the experiment obtained at $h\nu = 34$ eV and triangles for experiments obtained at $h\nu = 9$ eV); the dashed lines are a guide to the eye. (c) Theoretical bulk band dispersion without SOC effects along the ΓL high-symmetry line of the fcc structure. The inset shows the correspondence of the bulk and surface fcc Brillouin zones. (d) Theoretical bulk band dispersion without SOC effects along the ΓA high-symmetry line of hcp structure. The inset shows the correspondence of the bulk and surface hcp Brillouin zones.

discussed in Refs. [41,42]. In our case the deepest QWS converges to the band edge that can be estimated to be at 130 meV binding energy, thus indicating that bulk-related states form an electron pocket near $\overline{\Gamma}$. The discontinuities that QWSs present at about 0.2–0.3 Å^{-1} derive from the interaction with bulk band edges of Mo(110) [43], as also observed for other systems and comparable film thickness [44]. The origin of the band doubling close to the 0.55 Å^{-1} in

the 32 and 42 ML films (white arrows) will be addressed below.

Our experimental data near the Fermi energy can be compared with the results of DFT calculations. In both fcc and hcp structures the edges of bulk states that project onto $\overline{\Gamma}$ (i.e., states along ΓL for fcc and along ΓA for hcp) are above the Fermi energy [black curves in Figs. 1(c) and 1(d)], in agreement with previous calculations [24,25,28,30–32]. Strain and SOC effects induce minor changes in the band structure at the Fermi energy (see Refs. [24,25] and Supplemental Material, Sec. I and Figs. S1 and S2 [45]). As proposed in an earlier work on Yb [25], one can obtain a good agreement between theory and experiment by tuning the position of the unoccupied d bands. Indeed, the experimental band structure of Yb is similar to those of fcc Ca(111) and hcp Mg(0001) [46,47], which have higher d band and an electron pocket located at the L and Γ bulk points, respectively [2,5]. We applied the Hubbard U correction to the d orbitals of Yb: Since the conduction band consists mainly of d states, the effect of the U_d is similar to the one induced by the self-energy correction, as already demonstrated for other elements of the lanthanide group [48]. Figures 1(c) and 1(d) show DFT calculations with $U_d = 4$ eV (red curves), with a p-like band crossing the Fermi level in both fcc and hcp structures, which correctly reproduces the electron pocket observed experimentally. These results are in agreement with the previously demonstrated predominant p character of the Yb states below the Fermi level [22].

Before discussing in detail the electronic structure of Yb, we briefly address the crystallographic structure of the thin films. Yb is known to undergo an hcp-fcc transition close to room temperature with a high degree of hysteresis and sensitivity to the strain and contamination [13–16]. Yb films grown at room temperature and post-annealed at $T = 465$ K on Mo(110) and W(110) were shown to have an fcc structure [17,40]. On the other hand, the ARPES data presented here shows that the growth at room temperature and without annealing occurs in the hcp structure, similarly to Yb films grown on graphite [24]. This is proven by simple symmetry considerations of the bulk hcp and fcc reciprocal zone and of the way the bulk states are projected on the surface Brillouin zone [Figs. 1(c) and 1(d)]. In the fcc structure the L point is projected on the $\overline{\Gamma}$ and $\overline{M}$ points of the (111) surface [Fig. 1(c)]. Hence, electronic states with the same binding energy must be observed at $\overline{\Gamma}$ and at $\overline{M}$ (as can also be seen in Supplemental Material, Sec. I and Fig. S3). This is in contrast with the ARPES data for the Yb films, in which no states are seen close to the Fermi level at $\overline{M}$. As an example, Fig. 2(a) shows ARPES spectra for a 29-ML Yb film along the $\overline{K}\,\overline{\Gamma}\,\overline{M}\,\overline{K}$ path. Instead, in the hcp structure the $\overline{\Gamma}$ and $\overline{M}$ points of the (0001) surface are projections of different paths of the bulk Brillouin zone, namely, ΓA and ML [Fig. 1(d)], in agreement with the ARPES data.

Figures 2(b)–2(d) show DFT slab results for a 24-ML freestanding hcp Yb film. As expected, without U_d correction there is no electron pocket at $\overline{\Gamma}$ [see Fig. 2(b)]. The inclusion of U_d moves the QWSs at $\overline{\Gamma}$ below the Fermi level and they acquire nearly parabolic shapes [Fig. 2(c)], in agreement with ARPES data [Fig. 2(a)]. Additionally, a hole pocket emerges between $\overline{\Gamma}$ and $\overline{M}$. The inclusion of SOC effects results in a splitting of several states with surface character [Fig. 2(d)],

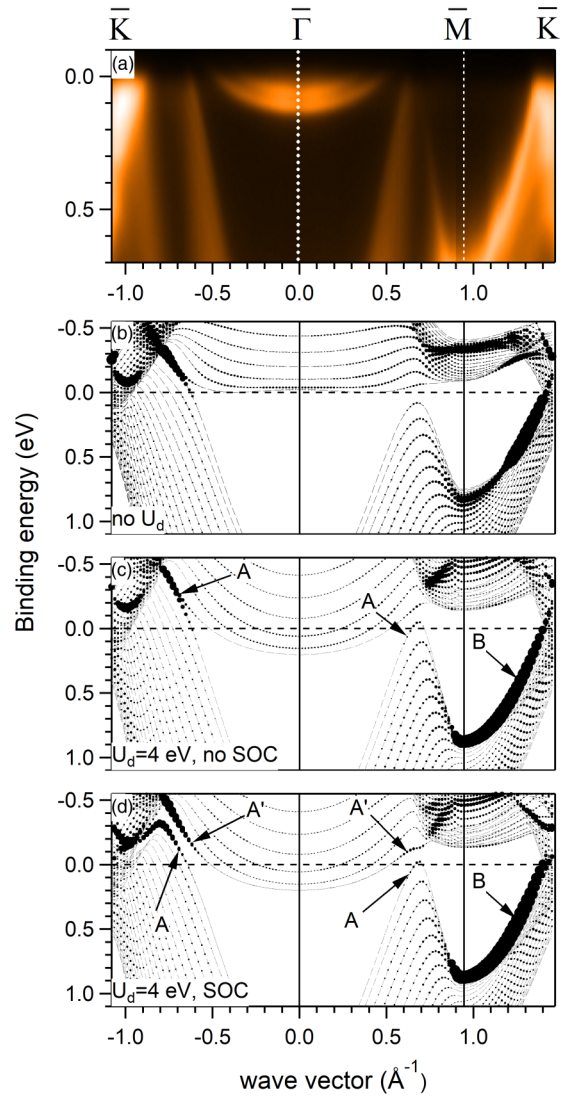

FIG. 2. (a) Photoemission intensity map along the $\overline{K}\,\overline{\Gamma}\,\overline{M}\,\overline{K}$ of a 29-ML Yb film for $h\nu = 34$ eV; (b),(c) Calculated surface band structure of 24-ML Yb(0001) film; symbol size is proportional to the $s + p + d$ character in the top two layers. (b) Without U_d, no SOC; (c) with $U_d = 4$ eV, no SOC; (d) with $U_d = 4$ eV, SOC. Black arrows indicate the surface states A, A', and B.

without significant energy shifts. A calculated band structure with a different U_d value is shown in Supplemental Material, Sec. II and Fig. S4. A similar effect of the U_d correction is expected also for fcc thin films. Several surface states marked A, A', and B [Fig. 2(d)] can be identified, while no surface state is observed at $\overline{\Gamma}$ (see also Supplemental Material, Sec. II and Fig. S5). As will be shown below, the A and A' states arise from topological properties of the bulk band structure.

Figures 3(a) and 3(b) show the calculated bulk band structure of hcp Yb along $K\Gamma MK$ high-symmetry lines in the limit of zero SOC without and with U_d, respectively. We notice that the band structure is strongly modified by the inclusion of U_d, inducing band crossings along ΓM, which otherwise are absent. As a result, there are two band crossings with s-p band inversion along the ΓK and ΓM directions [black arrows in Fig. 3(b) and red/blue circles in Figs. 3(c) and 3(d)] that

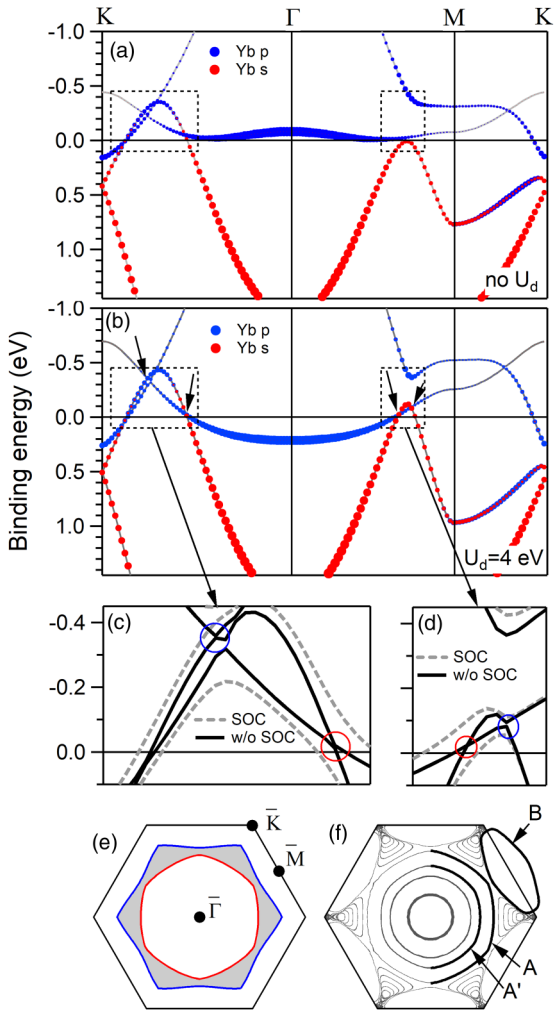

FIG. 3. (a),(b) DFT bulk band structure of hcp Yb along $K\Gamma MK$ with orbital projections without SOC (a) without U_d and (b) with $U_d = 4$ eV. (c),(d) Zooms on the band crossing without (black solid) and with (gray dashed) SOC included. Red (blue) circles indicate band crossings with an integral of the Berry curvature around the nodal line corresponding to $-\pi$ $(+\pi)$. (e) Surface Brillouin zone with a shaded region indicating the $k_\parallel$ distribution of the π Zak phase. (f) DFT + U_d constant energy cut taken at Fermi level for a 24-ML film with SOC included corresponding to the same slab with surface band structure shown in Fig. 2(d). Thicker lines mark the surface states A, A', and B.

extend over the Brilloiun zone and give rise to two DNLs. The Berry phase integrated around the loop in k space enclosing the DNL marked by the red (blue) circle is $-\pi$ $(+\pi)$. These DNLs are different from those in hcp Be and Mg, where the s-p band inversion occurs at Γ and only one DNL is present, and more similar to that of fcc Ca [2,5]. Indeed, there are two closely lying concentric DNLs. The DNL marked by the red color lies very close to the Fermi energy, resulting in a nearly flat contour, as in Ca(111). The projection of the two DNLs onto the (0001) surface is schematically shown in Fig. 3(e) by red and blue lines. The gray shaded region between them, indicating a range of states where the band inversion occurs and corresponding to a Zak phase $= \pi$ [2], does not include any time-reversal invariant momenta. Additionally, the SOC opens up a sizable gap at the Fermi level, as can be seen in Figs. 3(c) and 3(d). Therefore, no DNL can be directly observed [2]. In contrast, for the Yb in the fcc structure the inclusion of U_d induces almost no change in the topology of the DNL with respect to the band structure calculated without U_d (see Supplemental Material, Sec. I and Figs. S1 and S2).

In analogy to the Ca(111) surface, we can identify the DNL-related TSSs in Yb(0001). Without SOC we can observe a state A [Fig. 2(c)], which crosses the Fermi level once along $\overline{\Gamma K}$ and twice along $\overline{\Gamma M}$ (see also Supplemental Material, Sec. II and Fig. S5). Differently from the Ca(111) TSS, without SOC this state is located inside the bulk projected states. With the inclusion of SOC, A splits into two states A and A' [Fig. 2(d)], so along the $\overline{\Gamma K}$ direction the state A falls inside the bulk band gap, while along $\overline{\Gamma M}$ both the states are resonances. Figure 3(f) shows a calculated Fermi surface of 24-ML Yb(0001) film, corresponding to the band structure reported in Fig. 2(d). Three concentric contours in the center correspond to the electron pocket. We mark by thicker lines the contours corresponding to A and A' surface states: A' coincides with the outer of the QWSs in the center and A results in a nearly circular shape surrounding A'. Similar TSSs were reported on the surfaces of Ca(111) and Be(0001) [2,5]. The states A and A' acquire this circular shape only with U_d inclusion, which induces hole and electron pockets along the $\overline{\Gamma M}$ direction. The state B, which is an ordinary surface state, not related to the DNL, forms oval shapes surrounding the $\overline{M}$ points. Similarly to Ca(111), the states A and A' are not topologically protected (Supplemental Material, Sec. III and Fig. S6) [2,5]. A flattening of the bands would lead to disappearing of the DNL and therefore of the states A and A'.

Experimental evidence for all three surface states is provided in Fig. 4(a) showing the experimental Fermi surface. We overlap it with the calculated Fermi surface in panel (b). We notice a very good agreement between the theory and experiment. The crosslike features close to $\overline{K}$ derive from the state B. The broad intensity in the center is related to the QWSs and the state A'. We can also observe a sharp and intense circular contour whose position matches the state A. We notice that the intensity of the contour is higher when it approaches the $\overline{\Gamma K}$ direction, where according to the calculations the state A is located inside a gap. Figure 4(c) shows a zoom on the ARPES data close to the $k_\parallel$ position of contour A for several film thicknesses along $\overline{\Gamma K}$. As one can see this state remains at the same position for different film thicknesses in accord with its surface origin. The state A' can be observed in Fig. 1(a) as a doubling of the QWSs at approximately 0.55 Å^{-1}. The doubling is clear for 32-ML films, becoming smaller in 42 ML and disappearing for thicker films. We can notice the states A and A' also along the $\overline{\Gamma M}$ direction, where for relatively thin films there are two states just above the Fermi level which remain at the same $k_\parallel$ position (Supplemental Material, Sec. IV and Fig. S7). The state B, in turn, can be clearly seen in Fig. 2(a) as a bright feature along the $\overline{MK}$ direction.

As a last point, our study revisits the low-energy electronic structure of Yb and can help to reinterpret the electronic and transport properties of this material, as well as suggests novel ones. In particular, the self-energy correction reveals new topological properties of the poorly explored

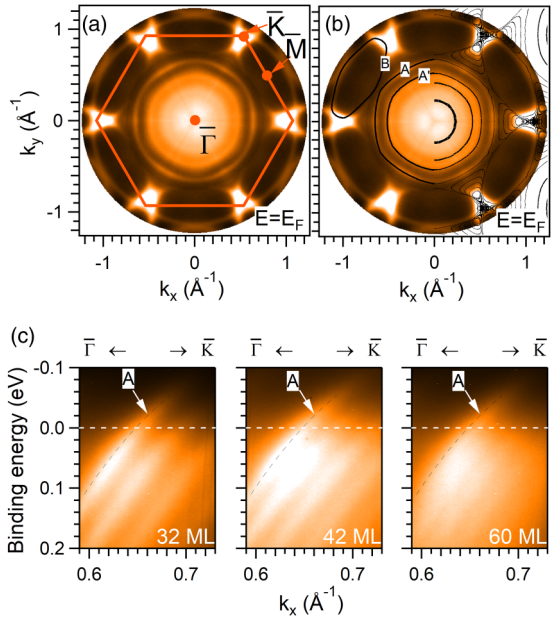

FIG. 4. (a) Constant energy cuts on a 29-ML Yb film with 34 eV photon energy taken at E_F. (b) The same, overlapped with DFT calculated Fermi surface from Fig. 3(f). (c) ARPES maps along the $\bar{\Gamma}\bar{K}$ direction for different thicknesses as indicated, with photon energy 9 eV. The dashed lines are guides to the eye.

hcp Yb. The two DNLs have π Berry phase, are gapped along all the momentum space due to large SOC, and are located very close to the Fermi level. These band structure properties are important for the spin Hall effect: as recently reported, multiple DNLs together with gap opening due to large SOC lead to large spin Hall conductivity [3,4]. The π Zak phase, in turn, leads to surface polarization charge and can result in substantial deformation of the lattice structure, which needs be explored [2]. Finally, the existence of the electron pocket in the band structure of fcc Yb was previously hypothesized in order to explain the resistivity and Hall data and phase transitions in Yb [14,25]. Also, the recently reported semimetal-semiconductor transition [11], pressure-induced superconductivity [12], and the lifetimes of excited electrons in Yb [31,32] were analyzed on the basis of rather different bulk band structure with no electron pocket at L and should be revisited. In general, our results indicate that in the calculation of Yb compounds, self-energy effects are more important than previously assumed.

IV. CONCLUSIONS

We have studied the electronic structure of hcp Yb by ARPES and DFT. ARPES evidences an electron pocket at $\bar{\Gamma}$ that can be reproduced by DFT calculations only by taking into account self-energy corrections on the d states. We furthermore discovered two Dirac nodal lines with a $\pm\pi$ Berry phase near the Fermi level, which emerge when spin-orbit interaction is neglected. The same approach predicts that an electron pocket forms at $\bar{\Gamma}$ also in fcc Yb. Dirac nodal line–related topological surface states predicted by theory are experimentally confirmed by ARPES. These unraveled topological properties open a pathway for exploring and understanding novel transport properties in this material.

ACKNOWLEDGMENTS

We gratefully acknowledge the computing resources on the supercomputer JURECA at the Jülich Supercomputing Centre (JSC). S.B. acknowledges financial support from the Deutsche Forschungsgemeinschaft (DFG) through the Collaborative Research Center SFB 1238 (Project No. C01). We acknowledge EUROFEL-ROADMAP ESFRI of the Italian Ministry of Education, University and Research, and the Convenzione Operativa "Tecnologie quantistiche per lo studio di sistemi alla nanoscala rilevanti alla realizzazione di applicazioni sensoristiche biomedicali, magnetiche ed elettroniche" between ISM-CNR and Dipartimento di Scienze of the University "Roma Tre."

[1] A. A. Burkov, M. D. Hook, and L. Balents, Phys. Rev. B **84**, 235126 (2011).
[2] M. Hirayama, R. Okugawa, T. Miyake, and S. Murakami, Nat. Commun. **8**, 14022 (2017).
[3] Y. Sun, Y. Zhang, C.-X. Liu, C. Felser, and B. Yan, Phys. Rev. B **95**, 235104 (2017).
[4] W. Hou, J. Liu, X. Zuo, J. Xu, X. Zhang, D. Liu, M. Zhao, Z.-G. Zhu, H.-G. Luo, and W. Zhao, npj Comput. Mater. **7**, 37 (2021).
[5] R. Li, H. Ma, X. Cheng, S. Wang, D. Li, Z. Zhang, Y. Li, and X.-Q. Chen, Phys. Rev. Lett. **117**, 096401 (2016).
[6] R. Li, J. Li, L. Wang, J. Liu, H. Ma, H.-F. Song, D. Li, Y. Li, and X.-Q. Chen, Phys. Rev. Lett. **123**, 136802 (2019).
[7] P. T. Sprunger, L. Petersen, E. W. Plummer, E. Lægsgaard, and F. Besenbacher, Science **275**, 1764 (1997).
[8] J. W. McCaffrey, D. A. Papaconstantopoulos, and J. R. Anderson, Solid State Commun. **8**, 2109 (1970).
[9] D. B. McWhan, T. M. Rice, and P. H. Schmidt, Phys. Rev. **177**, 1063 (1969).
[10] I. Vobornik, J. Fujii, M. Mulazzi, G. Panaccione, M. Hochstrasser, and G. Rossi, Phys. Rev. B **72**, 165424 (2005).
[11] C. Enderlein, M. Fontes, E. Baggio-Saitovich, and M. A. Continentino, J. Magn. Magn. Mater. **398**, 270 (2016).
[12] J. Song, G. Fabbris, W. Bi, D. Haskel, and J. S. Schilling, Phys. Rev. Lett. **121**, 037004 (2018).
[13] E. Bucher, P. H. Schmidt, A. Jayaraman, K. Andres, J. P. Maita, K. Nassau, and P. D. Dernier, Phys. Rev. B **2**, 3911 (1970).
[14] J. Alderson and C. Hurd, Solid State Commun. **11**, 1245 (1972).
[15] F. X. Kayser, Phys. Status Solidi A **8**, 233 (1971).
[16] G. A. Lenkov, A. E. Shitov, A. T. Burkov, and M. P. Volkov, Semiconductors **53**, 1853 (2019).
[17] M. E. Dávila, S. L. Molodtsov, M. C. Asensio, and C. Laubschat, Phys. Rev. B **62**, 1635 (2000).

[18] G. Brodén, S. B. M. Hagström, and C. Norris, Phys. Rev. Lett. **24**, 1173 (1970).
[19] G. Brodén, S. B. M. Hagström, and C. Norris, Phys. Kondens. Materie **15**, 327 (1973).
[20] F. Patthey, J.-M. Imer, W.-D. Schneider, H. Beck, Y. Baer, and B. Delley, Phys. Rev. B **42**, 8864 (1990).
[21] F. Offi, S. Iacobucci, L. Petaccia, S. Gorovikov, P. Vilmercati, A. Rizzo, A. Ruocco, A. Goldoni, G. Stefani, and G. Panaccione, J. Phys.: Condens. Matter **22**, 305002 (2010).
[22] F. Offi, P. Vilmercati, L. Petaccia, S. Gorovikov, A. Ruocco, M. I. Trioni, A. Rizzo, A. Goldoni, G. Stefani, G. Panaccione, S. Iacobucci, Phys. Rev. B **85**, 115108 (2012).
[23] G. Rossi and A. Barski, Solid State Commun. **57**, 277 (1986).
[24] Y. Wu, W. Zhang, Y. Fang, S. Lu, L. Wang, P. Li, Z. Wu, Z. Xiao, C. Cao, X. Wang, F. S. Li, Y. Yin, T. C. Chiang, Y. Liu, Phys. Rev. B **104**, L161402 (2021).
[25] G. Johansen and A. Mackintosh, Solid State Commun. **8**, 121 (1970).
[26] D. Wegner, A. Bauer, and G. Kaindl, Phys. Rev. Lett. **94**, 126804 (2005).
[27] D. Wegner, A. Bauer, and G. Kaindl, Jpn. J. Appl. Phys., Part 1 **45**, 1937 (2006).
[28] O. Jepson and O. Anderson, Solid State Commun. **9**, 1763 (1971).
[29] M. Bodenbach, A. Höhr, C. Laubschat, G. Kaindl, and M. Methfessel, Phys. Rev. B **50**, 14446 (1994).
[30] Y. Kubo, J. Phys. F **17**, 383 (1987).
[31] A. Marienfeld, M. Cinchetti, M. Bauer, M. Aeschlimann, V. Zhukov, E. Chulkov, and P. Echenique, J. Phys.: Condens. Matter **19**, 496213 (2007).
[32] V. P. Zhukov, E. V. Chulkov, P. M. Echenique, A. Marienfeld, M. Bauer, and M. Aeschlimann, Phys. Rev. B **76**, 193107 (2007).
[33] L. Petaccia, P. Vilmercati, S. Gorovikov, M. Barnaba, A. Bianco, D. Cocco, C. Masciovecchio, and A. Goldoni, Nucl. Inst. Meth. Phys. Res. A **606**, 780 (2009).
[34] N. Mårtensson, A. Stenborg, O. Björneholm, A. Nilsson, and J. N. Andersen, Phys. Rev. Lett. **60**, 1731 (1988).
[35] Y. S. Dedkov, D. V. Vyalikh, M. Holder, M. Weser, S. L. Molodtsov, C. Laubschat, Y. Kucherenko, and M. Fonin, Phys. Rev. B **78**, 153404 (2008).
[36] For a method description, see www.flapw.de.
[37] J. P. Perdew, K. Burke, and M. Ernzerhof, Phys. Rev. Lett. **77**, 3865 (1996).
[38] H. Krakauer, M. Posternak, and A. J. Freeman, Phys. Rev. B **19**, 1706 (1979).
[39] Q. Wu, S. Zhang, H.-F. Song, M. Troyer, and A. A. Soluyanov, Comput. Phys. Commun. **224**, 405 (2018).
[40] M. E. Dávila, S. L. Molodtsov, J. Avila, C. Laubschat, and M. C. Asensio, J. Appl. Phys. **93**, 5075 (2003).
[41] N. J. Speer, M. K. Brinkley, Y. Liu, C. M. Wei, T. Miller, and T.-C. Chiang, Europhys. Lett. **88**, 67004 (2009).
[42] T.-C. Chiang, Surf. Sci. Rep. **39**, 181 (2000).
[43] S. Chernov, K. Medjanik, C. Tusche, D. Kutnyakhov, S. Nepijko, A. Oelsner, J. Braun, J. Minár, S. Borek, H. Ebert *et al.*, Ultramicroscopy **159**, 453 (2015), special issue: LEEM-PEEM 9.
[44] P. Moras, D. Topwal, P. M. Sheverdyaeva, L. Ferrari, J. Fujii, G. Bihlmayer, S. Blügel, and C. Carbone, Phys. Rev. B **80**, 205418 (2009).
[45] See Supplemental Material at http://link.aps.org/supplemental/10.1103/PhysRevB.104.195138 for additional DFT calculations and ARPES data.
[46] F. Schiller, M. Heber, V. D. P. Servedio, and C. Laubschat, Phys. Rev. B **70**, 125106 (2004).
[47] F. Schiller and C. Laubschat, Phys. Rev. B **74**, 085109 (2006).
[48] P. Larson and W. R. L. Lambrecht, J. Phys.: Condens. Matter **18**, 11333 (2006).